CFD Letters www.cfdl.issres.net Vol. 6 (4) – December 2014

On RANS Modeling of Unconfined Swirl Flow

Arabi Radwan, Kamal A. Ibrahim[C], Ahmed Hanafy, Khalid M. Saqr

Mechanical Engineering Department, College of Engineering and Technology
Arab Academy for Science, Technology and Maritime Transport
P.O. Box 1029, Abu Quir, Alexandria – EGYPT

Received: 12/04/2014 – Revised 28/10/2014 – Accepted 17/12/2014

Abstract

This article presents numerical simulations of unconfined swirl flow. The Sydney swirl flow database was used as references for the boundary conditions and experimental validation. A number of RANS turbulence models were investigated in order to explore their potential in predicting axial and swirl velocity profiles of the swirl flow field. The numerical investigations showed that among the tested RANS models, the $k-\omega$ showed an acceptable performance in predicting the swirling flow features in both cases (low and high swirl level). The results also demonstrated that the $k-\omega$ model was able to provide a reasonably accurate prediction data that is in consistent with experimental measurements at most locations.

Keywords: Turbulence models, swirl flow, RANS, CFD, Sydney swirl burner

1. Introduction

1.1 Back ground

Swirling flow has received significant attentions in industrial applications recently. It has been widely adopted in several engineering applications either reacting or non-reacting systems so as to improve mixing or drying processes. The features offered by employing swirling flows make them an attractive option to be implemented in many practical engineering applications and industries. Using swirling flame, for example, in furnaces, diesel engines and gas turbine combustors is essential for enhancing flame stability and pollutant emission reduction. Swirling can be defined as the ratio of the tangential momentum flux to the axial momentum flux [1]. At high swirl intensities the angular-to-linear momentum exceeds a critical value causes an adverse axial pressure gradient in the flow direction. This pressure gradient is accompanied by a decrease in velocity [3]. This in turn causes a torroidal vortex-type recirculation zone to be established in the central region of the jet in the vicinity of the axis [2, 4]. This vortex- type also known as a vortex break down acts as storage of heat and mass. As the flow reversed as a result of recirculation zone some of the well mixed combustion products return to the flame fronts to mix with the fresh combustible mixture. Consequently, effective combustion is associated with such phenomenon. Furthermore, the flame length is reduced resulting in more stabilization combustion. Swirling flow can be also used in non-reacting cases such as spray dryer, and improving mixing process. However, there are some issues that can associate with swirling flow such as precessing vortex core (PVC) and jet precession. A review of the literature on

[C] Corresponding Author: Kamal A. Ibrahim Email: kamalabd49@hotmail.com

PII: S2180-1363(14)60159-X

swirling flow instabilities can be found in [4].These phenomena increase the instability and increase the complexity of understanding the nature physics or the behavior of both reacting and non-reacting swirling flow field.

Extensive experimental investigations have been performed to study both cold and reacting swirling flows in order to gain an in- depth understanding of the flow behavior and to discover its influence on the flow field structure see ref. [2, 5- 10]. These investigations reported most of the significant features of the flow. However, due to variety of engineering applications and a wide range of operating condition such as whether the flow is confined or not and different swirl levels, the experimental tool for further investigations is no more worthy as they are extremely expensive in terms of required equipment and time consumed. So the need for numerical investigations is essential for investigation such flows. Several computational approaches have been proposed to predict swirling flow features and fairly reasonable data comparable to experimental measurements were obtained. Some of these studies will be highlighted in the next section (literature review). It should be noted here a careful selection of the numerical tool is required in studying such flow, this mainly due to its complexity. Introduction of the high computer resources made it possible for Computational Fluid Dynamic (CFD) to be used as an efficient tool.

1.2 Literature Review

The Computational Fluid Dynamics (CFD) provides a promising numerical tool for investigation swirl flow either reacting or non-reacting case. Its powerful capability of predicting the insight physical phenomenon makes it an attractive option for design, optimization and emission reduction improvement of the combustion devices with efficient performance. Great deals of research studies showed encouraging results could be obtained with respect to the experimental data using mathematical modeling approaches such as Reynolds average Navier stokes (RANS) or Large eddy simulations(LES) methods with the aid of using the CFD. For examples, for the models based on RANS technique, Saqr et al. [11] performed a numerical study to examine the effect of hydrogen addition on flame temperature, structure and pollutant emissions computationally using FLUENT code. The numerical simulation was validated based on Sydney swirl burner. The realizable $k-\varepsilon$ and the steady laminar flamelet were used for turbulence closure and combustion models respectively. They reported a reduction in temperature as the hydrogen content increased; also variation of the flame length was observed. The production of NO was increased by the addition of hydrogen. A similar study conducted by Saqr at al. [12] to estimate the change in entropy generation in swirl stabilized flame (Sydney swirl burner) due to hydrogen addition to the fuel. The same computational methods are used as the previous study [11]. The only difference is the turbulence model in which they used a modified version of the proposed by Saqr et al. [13]. They revealed that an increase of the entropy generation occurred as a result of hydrogen enrichment. A numerical calculations based on RANS technique was carried out by Saqr et al.[14] so as to investigate the effect of free air stream turbulence intensity on the NOx and soot formation in turbulent combustion interaction.

Moreover, models based on RANS technique have been widely employed in predicting swirling flow in engineering applications. Although some studies revealed poor performance of such models mainly due to their isotropy properties, many studies show that careful choice of such models could provide good results compared to experimental evidence. For example, a numerical investigations conducted by Khademi et al. [15] in turbulent swirling can-combustor to estimate the performance of RANS turbulence models. Among the models used the eddy viscosity, RSM and SSG. The overall results showed that RSM and SSG show the best performance of predicting the axial and swirl velocity especially at low swirl number. However, these two models showed under prediction of the tangential velocity. It has been shown in term of low swirl value of that the Reynolds stress model produced a satisfactory prediction for axial and swirl prediction almost everywhere. Whereas among the eddy dissipation model the SST showed adequate predictions of the axial velocity except at the center line and poor prediction of

the swirl velocity. In case of high swirl number the RSM showed an improvement over the eddy viscosity models in terms of predicting the axial and the tangential velocity, though the $k-\varepsilon$ produced accurate agreement of the maximum velocity. The results also demonstrated that, though the eddy viscosity models were able to predict the central recirculation zone at high swirl case they were incapable of predicting its correct size. On the other hand, the RSM had shown the predictive capability of capturing the corner and the central recirculation zone in both flow cases. A similar study was carried out by Wegner et al. [16] to evaluate the performance of using the unsteady RANS (URANS) method in predicting an unconfined swirling with a precession vortex core phenomenon. The results showed the U-RANS could successfully capture the precession vortex core. Further investigations using RANS technique have been also implemented with the aid of computational fluid dynamics (CFD) to discover swirling flow features and the phenomena associated with such flow see ref [1,17-19].

With advancing capabilities of computer resources the ability of using sophisticated numerical technique such as the large eddy simulation (LES) is made affordable. A number of previous studies have demonstrated the application of LES technique to study swirling isothermal and combustion cases with successful degree obtained for predicting the flow characteristics in both cases. For examples, Yang et al.[20] used the LES to investigate two non-reacting cases selected form the Sydney swirling flame database with different swirl number (medium and high swirl cases). The results obtained showed that the LES results were able to capture the two regions of reverse –flow in case of the medium swirl level. Although there was some inaccurate data prediction at some location for the high swirl level in terms of axial velocity, the overall performance of the LES show a good agreement with experimental measurements. Stein et al. [21] examine the flow and mixing of two non-premixed cases selected from Sydney swirl burner (SM1 and SMH1) using LES technique. The steady laminar flamelet was applied to determine the chemical state in the flame. The results obtained showed excellent prediction achieved for the axial and tangential velocities of non-reacting case, also the quality of the predicted shear stresses where in a good agreement with experiments. While for the case of SMH1 the velocities showed a good agreement with experiments at upstream positions, however, further downstream the LES data showed a strong deviation compared to experimental work. The simulated mean and rms mixture fraction were reported to be predicted well, even though the vortex breakdown was not captured. However, slight deviations of the mixture of the mixture fraction resulted in incorrect predictions of species and temperatures. Another numerical simulation performed by Stein et al. [22] using combustion LES with emphasis placed here to the near flow field impact of boundary conditions. The analysis considered the mixture fraction and its variances prediction in the results. A good prediction of the axial and swirl velocities revealed to be achieved; also the mixture fraction predictions were reasonably good, despite some deficiencies at downstream locations. However, the overall results reported to be in a good agreement with experimental data with more grid refinement required to increase the accuracy.

Malalasekera et al. [23] has performed numerical calculations using LES with steady laminar flamelet model to investigate the features of SM1 swirl flame selected from Sydney swirl flames. They went to demonstrate that contribution of LES together with laminar flamelet model were successfully able to predict the swirling flow features, and thermo-chemical variables such as mixture fraction and temperature. El-asrag et al. [24] applied linear eddy mixing (LEM) in LES technique to investigate the swirl-stabilized flames (SM1 and SMA2) selected from the Sydney swirl burner. The results demonstrated that both the swirling flow features and the flame's structure were predicted correctly in both cases. Their final conclusions showed good agreements to experiments were achieved, and they went finally to support other findings of the capability of the LES as a potential tool for simulating swirl flames. James et al. [25] carried out a computational studies on Sandia/Sydney swirl burner (SM1 and SMA1 and Sandia/Darmstadt piloted jet diffusion flame (flame D) using the numerical tool of LES/FDF for the first time. The

overall predictions of the axial velocity and mean temperature were quiet well agree with the experimental data at several locations.

The LES technique has also received considerable attention by researchers not only for prediction the swirling flow features but also to investigate some problems associated with high swirl intensity such as jet precession and processing vortex core(PVC). It should be emphasized here that these phenomenon play a vital role in combustion stability. Numerous researches have been conducted recently to predict the occurrence of these phenomena with the aid of LES technique. For example, Dinesh et al. [26] simulate the Sydney swirl burner for two major cases. The two cases divided into seven cases with different values of swirl numbers to observe the effect of swirl number on flow behavior with an emphasis placed on vortex breakdown, recirculation and instability behavior. Their results revealed that the LES were capable of capturing the upstream recirculation zone and the downstream one (vortex breakdown). They had also been able to observe the existence of a central jet precession and the precession vortex core for all tested cases successfully. The most important finding from their studies showed that the LES has proved its capability in addressing the complex problems (instabilities) find in swirling jets. Dinesh et al. [27] also carried out another LES calculations for swirling flames selected from Sydney burner to demonstrate the LES efficiency in identifying the instabilities associated with swirling combustion flow. The results showed that LES technique could be used for swirl combustion applications, in particularly, to identify the unsteady flame properties and the flow field instabilities behavior.

In the light of the above argument, it can be seen that extensive experimental and theoretical studies in both reacting and non-reacting swirling have been performed over the past few decades. The LES technique can be deemed as a powerful numerical tool which is capable of providing consistent and excellent predictions compared to experimental measurements. Such model can be also used even in cases where there is no previous experimental data exist. However, they are relatively expensive in terms of computer resources and time requirements compared to the classical models based on RANS approach. While in practice engineering applications, engineers are not usually interested in accurate data that are closely matching the real measurements. Instead, moderate predictions with reasonable computational costs such as those models based on RANS technique would be fairly accepted. To this end, the present study is intended to perform an assessment performance of a classical models based on RANS technique in order to come up with a best model capable of predicting the flow field structure of swirling flow. The current investigation focuses on two non-reacting cases selected from Sydney swirl database, which has an unconfined flow features with a wide range of swirl levels and various operating conditions. Although similar studies have been carried out RANS method as in [15, 16] using, however, no one (up to my knowledge) has carried out investigations to evaluate the RANS models' performance on such burner. Another motivation behind using such burner is that extensive numerical studies have been conducted on this burner, such that the performance of successful model from the present test can be compared to other numerical tools like LES.

2. Mathematical Model

2.1. Governing equations [15]

Continuity equation:

$$\frac{\partial(\rho U_i)}{\partial x_i} = 0 \tag{1}$$

RANS equation:

$$\frac{\partial(\rho U_i U_j)}{\partial x_i} = -\frac{\partial P}{\partial x_i} + \frac{\partial}{\partial x_i}\left(\mu \frac{\partial U_i}{\partial x_j} - \rho\overline{u_i u_j}\right) \tag{2}$$

where $\rho\overline{u_i u_j}$ identified as the Reynolds stresses term and they are unknown. These stresses will be in subsequent section in order to close the system equations.

2.2. Turbulence model

Two sets of turbulence models are employed under this simulation studies to close the closure problem resulted from equation 2, which are the two equation eddy viscosity models and the RSM. In eddy viscosity models, the Reynolds stress tensor is linearly related to the mean strain rate [28, 29], as:

$$-\rho\overline{u_i u_j} = 2\mu_t S_{ij} - \frac{2}{3}\rho k \delta_{ij} \quad (3)$$

Where S_{ij} is the mean strain rate formulated as:

$$S_{ij} = \frac{1}{2}\left(\frac{\partial U_i}{\partial x_j} + \frac{\partial U_j}{\partial U_i}\right) \quad (4)$$

2.2.1 The standard $k-\varepsilon$

The, eddy viscosity, turbulent kinetic energy and its dissipation rate are obtained from the following transport equations, respectively:

$$\mu_t = C_\mu \rho \frac{k^2}{\varepsilon} \quad (5)$$

$$\frac{\partial(\rho U_j k)}{\partial x_j} = \frac{\partial}{\partial x_j}\left(\left(\mu + \frac{\mu_t}{\sigma_k}\right)\frac{\partial k}{\partial x_j}\right) + 2\mu_t S_{ij} S_{ij} - \rho\varepsilon \quad (6)$$

$$\frac{\partial(\rho U_j \varepsilon)}{\partial x_j} = \frac{\partial}{\partial x_j}\left(\left(\mu + \frac{\mu_t}{\sigma_\varepsilon}\right)\frac{\partial \varepsilon}{\partial x_j}\right) + 2C_{1\varepsilon}\frac{\varepsilon}{k}\mu_t S_{ij} S_{ij} - C_{2\varepsilon}\rho\frac{\varepsilon^2}{k} \quad (7)$$

The model constants, which are determined from experiments, are shown in table 1.

TABLE 1.THE MODELS' COEFFICIENTS

	C_μ	$C_{1\varepsilon}$	$C_{2\varepsilon}$	σ_k	σ_ε
Standard $k-\varepsilon$	0.09	1.44	1.92	1	1.3
Realizable $k-\varepsilon$		C_1	C_2	σ_k	σ_ε
	-	-	1.9	1	1.2
Standard $k-\omega$	α	β	β^*	σ	σ^*
	5/9	3/40	9/100	1/2	1/2

RSM	C_μ	C_1	C_2	C_1'	C_2'	$C_{1\varepsilon}$	$C_{2\varepsilon}$	σ_k	σ_ε
	0.09	1.8	0.6	0.5	0.3	1.44	1.92	1	1.3

2.2.2 The realizable $k-\varepsilon$

The realizable $k-\varepsilon$ differs from the standard $k-\varepsilon$ model in two ways which are; new formulations for eddy viscosity as well as a new transport equation for dissipation rate are introduced. However, the turbulent kinetic energy in this model has the same form as that in the standard model [29, 30].

$$\frac{\partial(\rho U_j \varepsilon)}{\partial x_j} = \frac{\partial}{\partial x_j}\left(\left(\mu + \frac{\mu_t}{\sigma_\delta}\right)\frac{\partial \varepsilon}{\partial x_j}\right) + C_1\rho S_\varepsilon - C_2\rho\frac{\varepsilon^2}{k+\sqrt{\nu\varepsilon}} \quad (8)$$

While C_μ is not constant and can be calculated as:

$$C_\mu = \frac{1}{A_o + A_s U^* \frac{k}{\varepsilon}} \quad (9)$$

Where

$$A_o = 4;\ \ U^* = \sqrt{S_{ij}S_{ij} + \Omega_{ij}\Omega_{ij}} \quad (10)$$

$$A_s = \sqrt{6}\,cos\left(\frac{1}{3}\,arccos\left(\sqrt{6}W\right)\right) \quad (11)$$

$$W = \frac{\sqrt{8}S_{ij}S_{jk}S_{ki}}{S^3} \quad (12)$$

The vorticity tensor expressed as:

$$\Omega_{ij} = \frac{1}{2}\left(\frac{\partial \overline{u_i}}{\partial x_j} - \frac{\partial \overline{u_j}}{\partial x_j}\right) \quad (13)$$

$C_1 = max\left(0.43, \frac{\eta}{\eta+5}\right),\ \eta = S\ \frac{k}{\varepsilon}, S = \sqrt{2S_{ij}S_{ij}}$

The rest of the model's constants are provided in table 1.

2.2.3 The standard $k-\omega$

The $k-\omega$ model was proposed by Wilcox incorporates modifications for low-Reynolds-number effects, compressibility, and shear flow spreading. The major advantage of this model compared to the standard $k-\varepsilon$ is related to its numerical stability; also it is very sensitive to the free steam boundary conditions [28-30]. The transport equation for the turbulent kinetic energy and the specific dissipation rate are expressed as:

$$\frac{\partial(\rho U_j k)}{\partial x_j} = \frac{\partial}{\partial x_j}\left(\left(\nu + \sigma^* \frac{k}{\omega}\right)\frac{\partial k}{\partial x_j}\right) + \tau_{ij}\frac{\partial u_i}{\partial x_j} - \beta^* k\omega \quad (14)$$

$$\frac{\partial(\rho U_j \omega)}{\partial x_j} = \frac{\partial}{\partial x_j}\left(\left(\nu + \sigma \frac{k}{\omega}\right)\frac{\partial \omega}{\partial x_j}\right) + \alpha\frac{\omega}{k}\frac{\partial \overline{u_i}}{\partial x_j}\frac{\tau_{ij}}{\rho} - \beta\omega^2 \quad (15)$$

$$\varepsilon = B^*\omega k \quad (16)$$

2.2.4 Reynolds Stress Model (RSM)

The Reynolds stresses under this model are calculated based on their transport equation. The major advantage of the RSM over that two equation models is its capability of representing the highly anisotropic nature of the flow and accounts for swirl effect as well as stream line curvature [28, 29].

The transport equation s for the Reynolds stresses, $-\rho\overline{u_\iota u_j}$, can be expressed as:

$$\frac{\partial}{\partial x_k}\left(\rho u_k \overline{u_\iota' u_j'}\right) = \frac{\partial}{\partial x_k}\left(\frac{\mu_t}{\sigma_k}\frac{\partial \overline{u_\iota' u_j'}}{\partial x_k}\right) + \frac{\partial}{\partial x_k}\left[\mu\frac{\partial}{\partial x_k}\left(\overline{u_\iota' u_j'}\right)\right] - \rho\left(\overline{u_\iota' u_j'}\frac{\partial u_j}{\partial x_k} + \overline{u_j' u_\iota'}\frac{\partial u_i}{\partial x_k}\right) + \Phi_{ij} - \frac{2}{3}\delta_{ij}\rho\varepsilon \quad (17)$$

The term on the left side of the above equation represents the convective term, and the terms on the right hand side represent the turbulent diffusion, molecular diffusion, stress production (P_{ij}), pressure strain (Φ_{ij}) and the dissipation, respectively.

The pressure strain term is simplified according to the model proposed by Gibson and Launder.

$$\Phi_{ij} = \Phi_{ij,1} + \Phi_{ij,2} + \Phi_{ij,w} \quad (17)$$

Where

$$\Phi_{ij,1} = -C_1\rho\frac{\varepsilon}{k}\left[\overline{u_\iota' u_j'} - \frac{2}{3}\delta_{ij}k\right] \quad (18)$$

$$\Phi_{ij,2} = -C_2\left[\left(P_{ij} - C_{ij}\right) - \frac{1}{3}\delta_{ij}(P_{kk} - C_{kk})\right] \quad (19)$$

$$\Phi_{ij,w} = C_1'\frac{\varepsilon}{k}\left(\overline{u_k' u_m'}\, n_k n_m \delta_{ij} - \frac{3}{2}\overline{u_\iota' u_k'}\, n_j n_k - \frac{3}{2}\overline{u_\iota' u_k'}\, n_j n_k\right)\frac{k^{3/2}}{C_{\iota\varepsilon d}} + C_2'\left(\phi_{km,2}\, n_k n_m \delta_{ij} - \frac{3}{2}\phi_{ik,2}\, n_j n_k - \frac{3}{2}\phi_{jk,2}\, n_j n_k\right)\frac{k^{3/2}}{C_{2\varepsilon d}} \quad (20)$$

The model of the dissipation rate term $\boldsymbol{\varepsilon}$ is the same as in the standard $\boldsymbol{k-\varepsilon}$ model

Where,

$C_l = {C_\mu^{3/4}}/{\kappa}$, and κ is the von Karman constant = 0.4187

The detailed description of the model can be found in [28-30].

3. Physical Model and Simulation Cases

3.1. Sydney swirling burner

The Sydney Swirl burner is selected for simulation purpose. The burner has a 50 mm diameter ceramic face bluff-body with a central jet tube of 3.6 mm in diameter. Surrounding the bluff body is a 60 mm diameter annulus with a 0.2 mm thick lip. Swirling flow comes out of the annulus which is 5 mm in width. The swirl is induced aerodynamically at air stream via three tangential ports (7 mm each) located at 300 mm upstream of the burner exit. The burner configuration is shown in fig.1 [31, 32]. To provide well-defined boundary conditions, the burner is placed in a square wind tunnel with a cross section of 130X130 mm2. More details can be found in [31, 32].

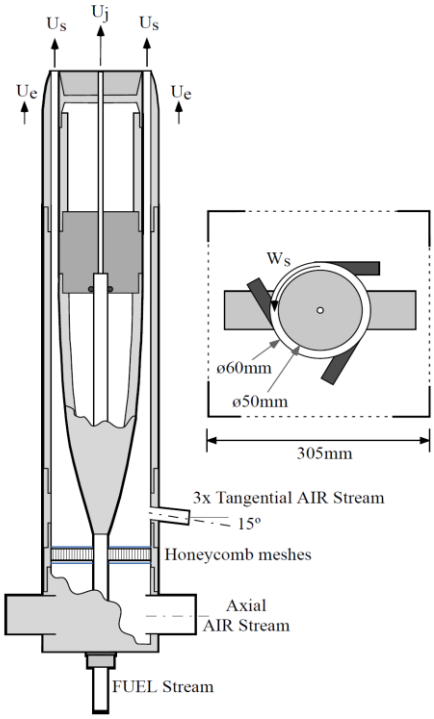

Figure1. Sydney swirl burner configuration. The figure is courtesy of [32,33]

3.2. Simulation cases

Two non-reacting cases are selected from Sydney database for simulation purpose. Each case has different swirl value (Sg=Ws/Us). They are identified as N29S054 and N16S159, referred to in the present article as a medium and high swirl level. Table 2 provides the flow configurations and the boundary conditions of each case [32]. The Reynolds number is defined as Re=Uj D/v, where D is the jet diameter.

TABLE 2. FLOW CONFIGURATION OF SIMULATED CASES

case	Fuel	Uj(m/s)	Us(m/s)	Ws(m/s)	Ue(m/s)	Sg	Re
N29S054	Air	66	29.7	16	20	0.54	59000
N16S159	Air	66	16.26	25.9	20	1.59	32400

4. Computational Approach

4.1. Computational domain

Because of symmetry only half of the flow is simulated. The 2D axisymmetric geometry and the grid generation technique are performed using Gambit version of 6.3. The numerical simulation are carried out on a discretised computational domain of Cartesian shape with dimensions of 150 mm x 300 mm , in X and Y directions, repecrively as shown in fig.2.

see the figure below (figure 2, all dimensions are in mm)

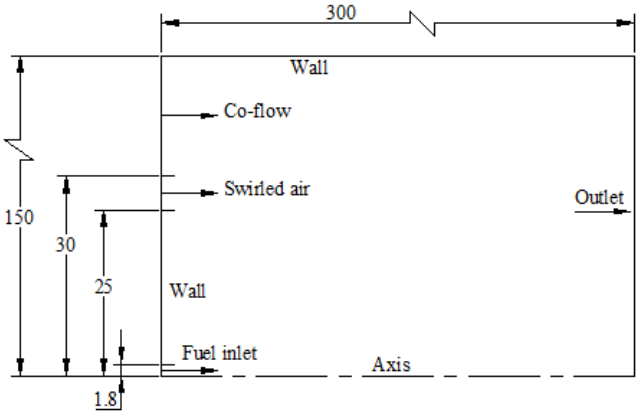

Figure 1: schematic diagram of the geometry used in the simulation. All dimensions in mm.

4.2. Numerical Solver parameters

The FLUENT code, which is based on the finite volume method, is employed for the numerical calculations of the governing equations. The Semi-Implicit Method for Pressure Linked Equations (SIMPLE) is applied for the pressure-velocity coupling [33]. The second order up wind is applied for the convection terms and standard method is used for the pressure discretization. The solution convergence is set to be 10^{-6} residual for all the parameters.

4.3. Grid Independence Study

A grid independence study had to be conducted first in order to provide an optimum grid resolution. Four mesh sizes system have been generated in a 2D domain to assess the computational mesh solution convergence. They are referred to as G1, G2, G3 and G4. The number of cells for the G1, G2, G3 and G4 are, 36000, 81900, 88600 and 101200 respectively. Experience from previous numerical simulations shows similar level of number of cells. Table 3, lists some of mesh sizes adopted in previous work generated after grid independence study.

Table 3. Grid size used in previous numerical studies

Author	Turbulence model	Grid size
Saqr [11]	Realizable $k-\varepsilon$	146,000 cells
Saqr[12]	$R_\varepsilon/k-\varepsilon$	9.3×10^4 cells
Yilmaz[1]	$k-\varepsilon$	63,450 nodes
Saqr[14]	$k-\varepsilon$	20×10^3 cells

Comparison of simulation results (line) obtained from the RSM model with experimental data (points) at station x/D=0.136 is shown in figure 3. It can be observed that the general trend of the predicted axial velocity profiles can be captured by the four generated grid systems. However, G3 provides excellent results that are consistent with their counterpart's experimental data.

It is worth mentioning that further refinement will no longer increase the accuracy; it would rather increase the computational time which in turn, make the numerical modeling more expensive. Therefore, the third grid (G3) system was adopted under this numerical simulation to obtain all the necessary data.

Figure 3 demonstrate the comparison of axial velocity profiles of the four generated grid compared against the experimental data, both are plotted with normalized radial profiles (normalized by burner radius, R= 25 mm). It can be observed form the figure below that G3 provides excellent results that are consistent with their counterpart's experimental data.

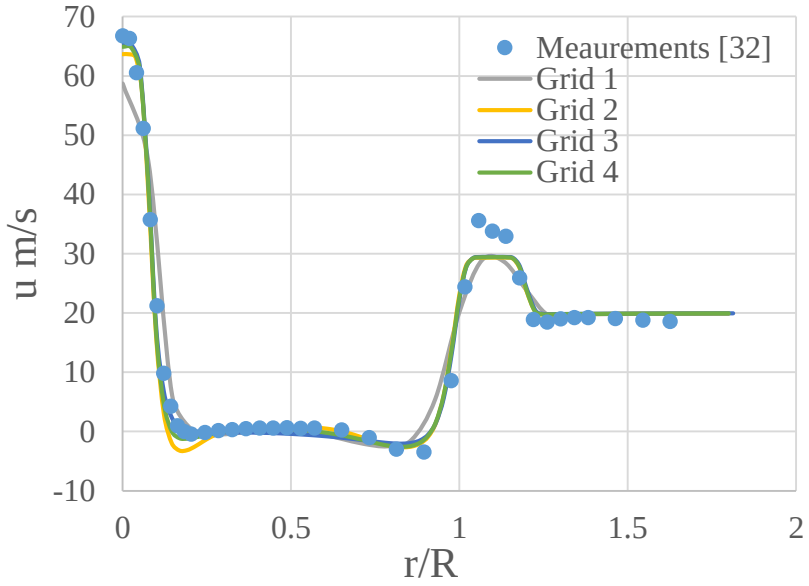

Figure 3: Radial profile of predicted axial velocity at location x=6.8 mm (x/D=0.136)

5. Results and discussion

This section compares the numerical data, obtained from the RANS models, with the measurements. The results will be discussed in two cases. Case 1 represents a quantitative analysis of axial velocity for both medium and high swirl levels (N29S054 & N16S159) while case 2 corresponds to the swirl velocity of both levels.

5.1. Axial velocity fields of both swirl intensities.

Quantitative comparisons of the axial velocity components for several axial stations (representing near, mid and far-field of the flow) are depicted in figure 4. The results clearly demonstrate that both the eddy viscosity models and the RSM are able to predict the axial velocity at regions near the inlet stations (i.e. x/D = 0.136 & 0.2). It can also be observed that, for the near stations, the axial velocity profiles of the turbulence models are comparable to each other and are in a good agreement with measurements for both swirl intensities.

However, as the flow progresses axially (downstream) these models (except the $k-\omega$) even the RSM fail to predict the axial velocity, though the rest of the RSM trend show a good agreement to experimental data. The major disagreement between the experiments and numerical calculations appeared at the center region, where they provide a poor performance of capturing the velocity of jet decays. The reason behind the deficiencies persistent of the eddy viscosity models, as has been reported in previous work [15], could be related to their isotropic nature, whereas the structure of the swirling flow is believed to be influenced by anisotropic turbulence. An interesting finding can be dedicated from the results is that the performance of the eddy viscosity models at high swirl value (right column) show an improvement over the lower one at most locations (starts from x/D=0.4 – 2).

More importantly, the RSM does not produce the most accurate data as was expected. According to the literature, the RSM provides better performance compared to eddy viscosity models, since its account for stream line curvature and swirling effect. However, for this case the RSM performance seems to be poor compared to $k-\omega$ model. It can be concluded the data obtained by the $k-\omega$ model are the most adequate predictions compared to the experimental data of [32]. Hence the $k-\omega$ model for this case and can be deemed as a good tool for analyzing the flow features.

Medium swirl level

High swirl level

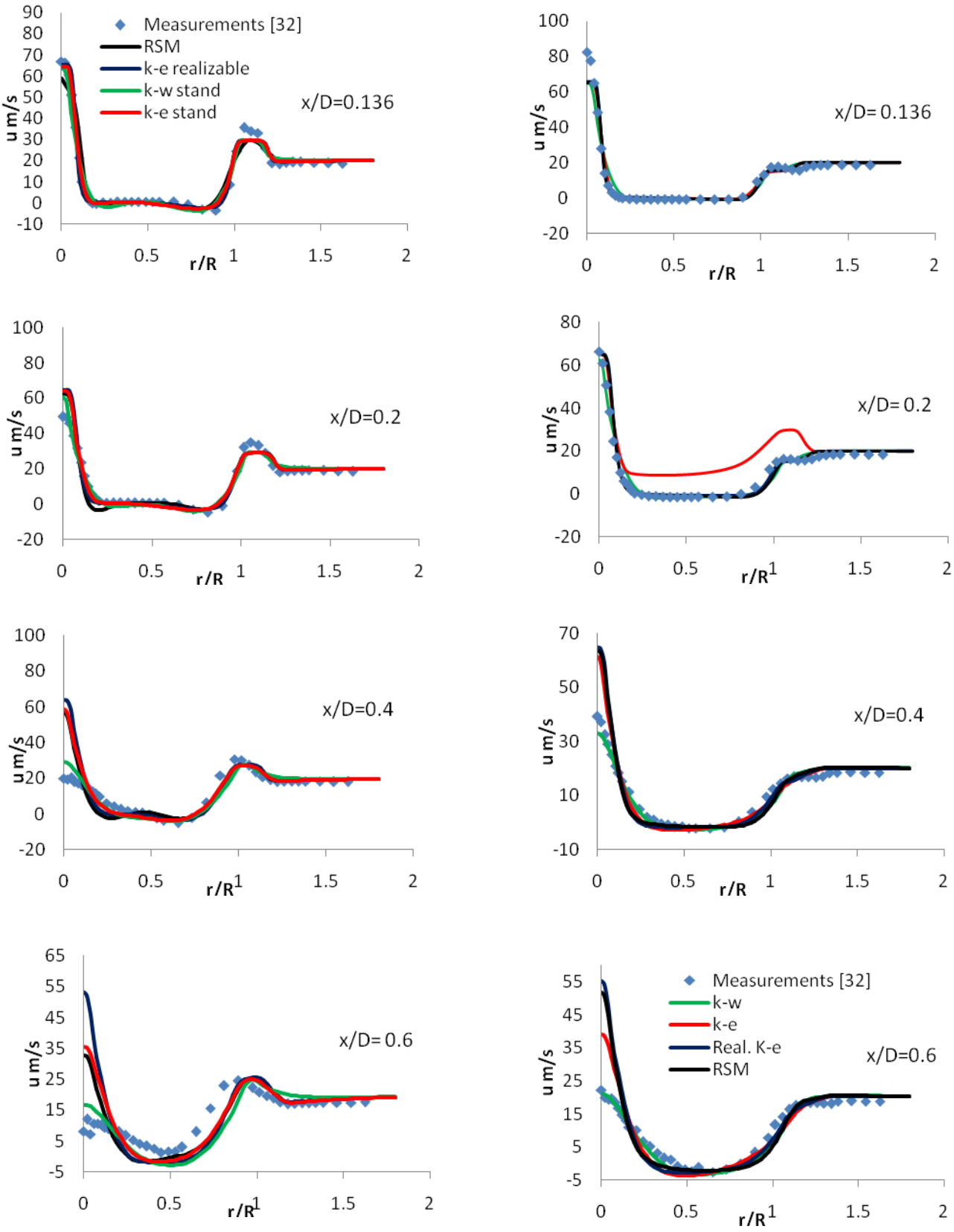

Figure 4. Radial profile of axial velocity distribution at different locations. Left column: medium swirl level (N29S054), right column: high swirl level (N16S159).

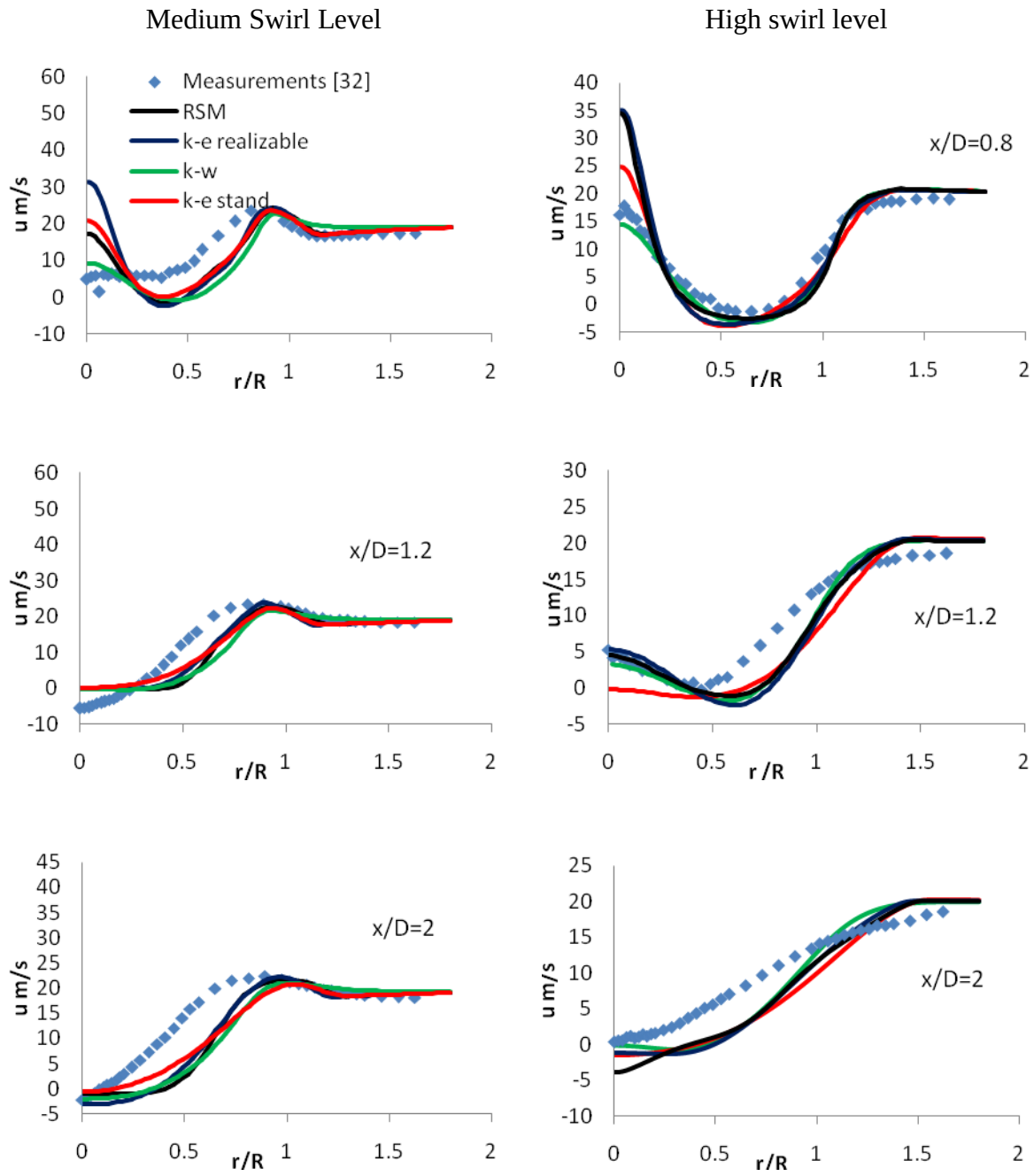

Figure 4. Radial profile of axial velocity distribution at different locations. Left column: medium swirl level (N29S054), right column: high swirl level (N16S159).

4.2 Swirl velocity fields of both swirl intensities

The computational results of the swirl velocity of both swirl levels are compared against experimental data, as shown in figure 5, for several axial stations. As can be observed, all the two-equation eddy viscosity models(except the $k-\varepsilon$) and the RSM produce a reasonable predictions at near stations (from x/D=0.136-0.4 mm) for both swirl levels while the $k-\varepsilon$ model in case of medium swirl condition shows a slight over prediction at these locations. The results demonstrate that, for the medium swirl level, the realizable $k-\varepsilon$ model markedly revealed better performance (with respect to the experimental data) over the other tested models at various locations covering the range from x/D= 0.136-1.2.

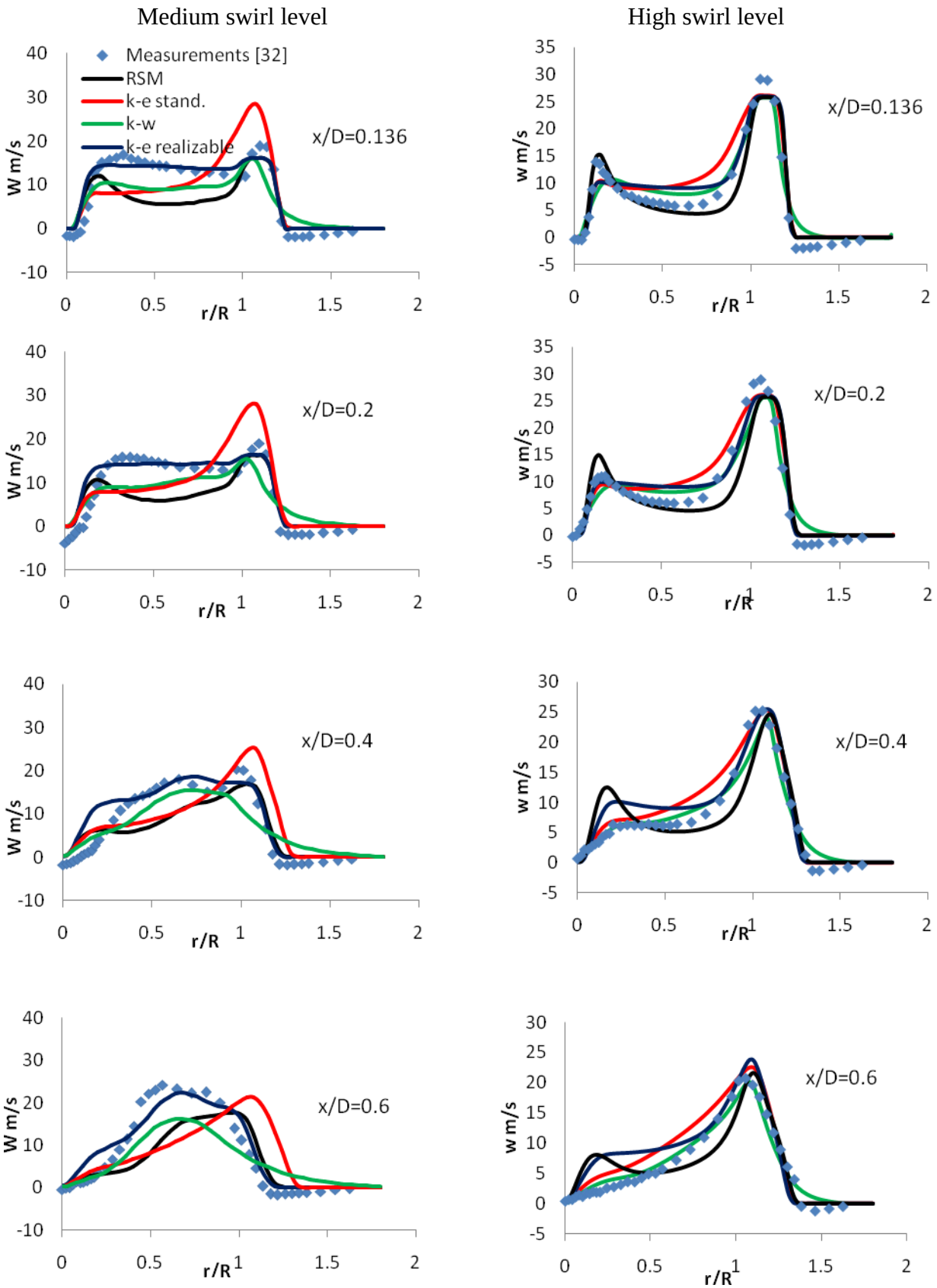

Figure 5. Radial profile of swirl velocity distribution at different locations. Left column: medium swirl level (N29S054), right column: high swirl level (N16S159).

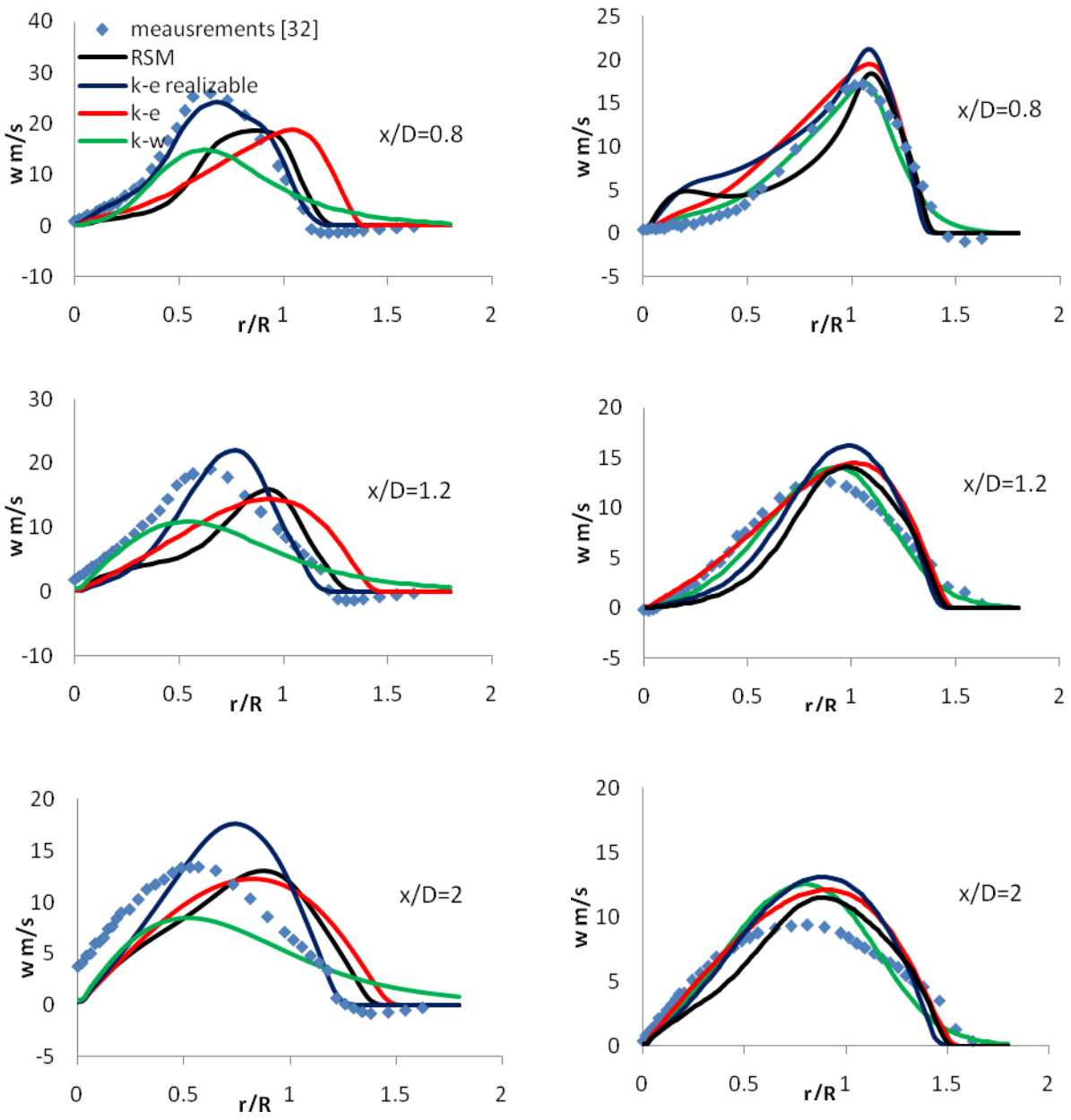

Figure 5. Radial profile of swirl velocity distribution at different locations. Left column: medium swirl level (N29S054), right column: high swirl level (N16S159).

The performance of $k-\omega$ shows a reasonable predictions of the swirl velocity profiles despite the fact that it slightly under predicted the maximum velocity in far regions. The other models show adequate predictions compared to measurements and a similar trend can be observed for the $k-\varepsilon$ and RSM at x/D=2.

For the high swirl level, on the other hand, the predicted swirl profiles of all the tested models are in good agreement with experimental data in shape and magnitude at most locations. The results demonstrate that the predicted velocity generated by the $k-\omega$ model quite accurately reproduced the measured profiles. It should be mentioned that, swirl velocity curves show a Rankin-type profile (combined forced vortex and free vortex), which is a characteristic of the swirling velocity profile. Such characteristic of the flow which cut through cross-sections x/D= 0.6-2 is being captured by all the models. It should be noted that such feature can be clearly observed in the high swirl level better than the medium case.

6. Conclusion

A numerical simulation test was performed to assess the ability of RANS models based on predicting the behavior of turbulent swirling flows. The objective was to produce a mathematical turbulence model that is capable of predicting the characteristics of swirling flow reasonably with moderate computational cost. Two non-reacting cases were selected from the Sydney swirl burner database for the assessment purpose. The main conclusions of the numerical investigations are summarized as:

- In comparison with all the tested model, the performance of the $k-\omega$ in predicting the axial and the swirl velocities in both swirl intensities show to be in a good agreement with experimental data. Although at medium swirl condition the realizable $k-\varepsilon$ show an improvement over the $k-\omega$ at some locations, the $k-\omega$ still provides satisfactory predictions.
- -It is found that the predicted profiles of both the eddy viscosity models and the RSM are in a reasonable agreement with measurements in terms of shape and magnitude in the strongly swirling flow. Moreover, significant improvements were observed from the tested model over the medium swirl case.
- -Although the RSM and the $k-\varepsilon$ show moderate predictions at some locations, their deficiencies were evident in the vicinity of the center line, where they fail to capture the jet velocity deceleration. On the other hand, the $k-\omega$ model showed a desirable capturing of this velocity which made it a superior over all the tested models.
- -The results also demonstrate that the tested models were able to reproduce the Rankin shape of the swirl velocity. The $k-\omega$ model performs well in capturing this phenomenon. Its performance also showed to be superior to any other models and even better than the medium swirl level.
- . In summary, among the tested two-equation eddy viscosity and RSM models the $k-\omega$ model shows a fairly accurate prediction data that is in consistent with experimental measurements at most locations. So such model can be used as a tool to provide the main characteristic of swirling for combustor similar to the Sydney burner configuration.

Nomenclature

Latin symbols

U_i, U_j, U_k	Mean velocity components
x_i, x_j, x_k	Space direction
$\overline{u_i u_j}$	Reynolds stresses
P	Pressure [Pa]
u_i, u_j, u_k	Velocity fluctuating components
k	Turbulent kinetic energy [m^2/s^2]
S_{ij}	Mean rate of strain tensor
Uj	Central jet velocity (m/s)
Us	The bulk axial velocity of the annulus (m/s)
Ws	The bulk tangential velocity (m/s)
Ue	The co-flow velocity of the wind tunnel
Sg	Swirl number, =Ws/Us
Re	Reynolds number

Greek symbols

τ_{ij}	Viscous stress tensor [N/m^2]
δ_{ij}	Kronecker operator
μ	Laminar viscosity [kg/m.s]
μ_t	Turbulent viscosity [kg/m.s]

μ_{eff}	Effective viscosity [kg/ m.s]
ε	Dissipation rate of k
ρ	Density [kg/m^3]
ν	Kinematic viscosity [Cm^2/s]
σ_k	Turbulent Prandtl number for k, =1
σ_ε	Turbulent Prandtl number for ε, =1.3
σ_δ	Turbulent Prandtl number for ε, =1.2
Ω_{ij}	Mean vorticity tensor
ω	Specific dissipation rate of
β, β^*, α	$k-\omega$ model based constants, = 3/40, 9/100, 5/9.
Φ_{ij}	Pressure strain term of Reynolds stress transport equation
κ	Von Karman constant = 0.4187

Subscripts

i	In x direction
j	In y direction
k	In z direction

References

[1] Yilmaz, İ., *Effect of Swirling Number on Combustion Characteristics in a Natural Gas diffusion Flames, Transactions of ASME*, Journal of Energy Resources Technology, 2013. 135: p. 0422041-0422048.

[2] Syred, N., N. A. Chigier, and J. Beer. *Flame Stabilization in Recirculation Zones of Jets with Swirl*, Department of Fuel and Chemical engineering, University of Sheffield, England.

[3] Stone, C., *Large-Eddy Simulation of Combustion Dynamics in Swirling flows*, PhD Thesis, 2003, Georgia Institute of Technology.

[4] Syred, N., *A review of oscillation mechanisms and the role of the precessing vortex core (PVC) in swirl combustion systems*, Progress in Energy and Combustion Science, 2006. 32: p. 93-161.

[5] Jufar, S. R., R.F. Huang, and C.M. Hsu. *Effect of swirl on flow and mixing of acoustically excited double-concentric jets*, Experimental Thermal and Fluid Science, 2013. 49: p.40-50.

[6] Valera-Medina, A., N. Syred, P. Bowen, and A. Crayford. *Studies of Swirl Burner Characteristics, Flame Length and Relative Pressure Amplitudes*, Transactions of ASME, Journal of Fluids Engineering, 2011. 133:p. 1013021-10130211.

[7] Al-Abdeli,Y. M., and A. R. Masri, *Recirculation and flow field regimes of unconfined non-reacting swirling flows*, Experimental Thermal and Fluid Science, 2003. 27: p. 655-665.

[8] Kalt, P. A., Y. M. Al-Abdeli, A. R. Masri, and R. S. Barlow. *Swirling turbulent non-premixed flames of methane: flow field and compositional structure*, Proceeding of the Combustion Institute, 2002. 29: p. 1913-1919.

[9] Masri, A.R., P. A. Kalt, and R.S. Barlow, *The compositional structure of swirled-stabilized turbulent nonpremixed flames*, Combustion and Flame, 2004. 137: p. 1-37.

[10] Zang, S. and B. Ge., *Technical brief: Predictions of flow field for circular-disk bluff-body stabilized flame investigated by large eddy simulation and experiments*, Transactions of ASME, Journal of Engineering for Gas turbines and Power, 2010. 132: p. 054503-0545036.

[11] Saqr, K. M. and B. Rohani., *Effect of hydrogen addition on the structure and polluatant emissions of a turbulent unconfined swirling flame*, International Communications in Heat and Mass transfer, 2012. 39: p. 681-688.

[12] Saqr, K. M. and M. A. Wahid., *Entropy Generation in Turbulent Swirl-Stabilized Flame: Effect of Hydrogen Enrichment, Department of mechanical engineering*, Applied Mechanics & Materials, 388: p.280-284.

[13] Saqr, K. M, H. A. Wahid, and M. M. Sies. *Numerical simulation of confined vortex flow using a modified $k-\varepsilon$ Turbulence model*, CFD letters, 2009. 1: p. 87-94.
[14] Saqr, K. M.,, *Effect of free stream turbulence on NOx and soot formation in turbulent diffusion CH4- air flames*, International Communications in Heat and Mass Transfer, 2010. 37: p. 611-617.
[15] Khademi, K. and M. Bairouk., *Assessment of the performance of RANS models for Simulating Swirling Flows in a Can- combustor*, The Open Aerospace Engineering Journal, 2008. 1: p. 8-27.
[16] Wenger, B. A. Maltsev, C. Schneider, A. Sadiki, A. Dreizler, and J. Janicka. *Assessment of unsteady RANS in predicting swirl flow instability based on LES and experiments*, International Journal of Heat and Flow, 2004. 25: p. 528- 536.
[17] Guo, B., T. A. Langrish, and D. F. Fletcher. *CFD simulation of precession in sudden pipe expansion flows with low inlet swirl*, Applied mathematical modeling, 2006. 26: p. 1-15.
[18] Jochmann, P., A. Sinigersky, M. Hehle, O. Schäfer, R.Koch, and H. Bauer. *Numerical simulation of a precessing vortex breakdown*, International Journal of Heat and fluid Flow, 2006. 27: p. 192-203.
[19] Jawarneh, A. and G. H. Vatistas., *Reynolds Stress Model in the Prediction of Confined Turbulent Swirling Flows*, Transactions of ASME, Journal of Fluids Engineering, 2006. 128: p.1377-1382.
[20] Yang, Y. and S. Kær., *Large –eddy simulation of the non-reactive flow in the Sydney swirl burner*, International Journal of Heat and Fluid flow, 2012. 36: p. 47- 57.
[21] Stein, O. and A. Kempf., *LES of the Sydney swirl flame series: A study of vortex breakdown in isothermal and reacting flows*, Proceeding of the combustion Institute, 2007. 31: p. 1755-1763.
[22] Stein, O. A. kempf, and J. Janicka. *LES of the Sydney swirl flame series: An initial investigation*, Combustion Science and Technology, 2007. 179: p. 173-189.
[23] Malalasekra, W. K. Ranga-Dinesh, S. S. Ibrahim, A. R. Masri. *LES of Recirculation and Vortex breakdown In swirling flames*, Combustion Science and Technology, 2008. 180: p. 809-832.
[24] El-Asrag, H. and S. Menon., *Large eddy simulation of bluff- body stabilized swirling non-premixed flames*, Proceeding of the Combustion Institute, 2007. 31: p.1747-1754.
[25] James, S., J. Zhu, and M. S. Anand. *Large eddy simulation of turbulent flames using the filtered density function model*, Proceeding of the Combustion Institute, 2007. 31: p.1737-1745
[26] Ranga-Dinesh, K.K.J. and M. P. Kirkpatrick., *Study of jet precession , recirculation and vortex breakdown in turbulent swirling jets using LES*, Computer & Fluids, 2009. 38: p.1232-1242.
[27] Ranga-Dinesh, K.K.J., K.W. Jenkins, M. P. Kirkpatrick, and W. Malalasekera. *Modelling of instabilities in turbulent swirling flames*, Fuel, 2010. 89: p.10-18.
[28] FLUENT theory and user guide.
[29] Dewan. A., Tackling Turbulent Flows in Engineering, Springer-Verlag Berlin Heidelberg, 2011. ISBN 978-642-14766-1.
[30] Saqr. M. K. and M. A. Wahid., *Comparison of Four Eddy –Viscosity Turbulence Models In the Eddy Dissipation Modeling of Turbulent Diffusion Flames*, International Journal of Applied Mathematics and Mechanics, 2011. 7: p. 1-18.
[31] Al-Abdeli, Y. and A. R. Masri., *Recirculation and flowfield regimes of unconfined non-reacting swirling flow*, Experimental Thermal and Fluid Science, 2003. 27: p.655-665.
[32] Al- Abdeli, Y., *Swirl Flow and Flames Database [online]*. Sydney University.
[33] Available from: http://sydney.edu.au/engineering/aeromech/thermofluids/swirl.htm [Accessed 10 November 2013].
[34] Jiyuan, T., Computational Fluid Dynamics, 2nd edition. A practical Approach.
[35] ISBN: 978-0-7506-8563-4